Kinetics of Fe(II)-Catalyzed Transformation of 6-line Ferrihydrite under Anaerobic Flow Conditions

LI YANG,*,† CARL I. STEEFEL,† MATTHEW A. MARCUS,‡ AND JOHN R. BARGAR§

Earth Sciences Division, Lawrence Berkeley National Laboratory, Berkeley, California 94720, Advanced Light Source, Lawrence Berkeley National Laboratory, Berkeley, California 94720, and Stanford Synchrotron Radiation Lightsource, Menlo Park, California 94025

Received March 10, 2010. Revised manuscript received May 24, 2010. Accepted June 4, 2010.

The readsorption of ferrous ions produced by the abiotic and microbially mediated reductive dissolution of iron oxy-hydroxides drives a series of transformations of the host minerals. To further understand the mechanisms by which these transformations occur and their kinetics within a microporous flow environment, flow-through experiments were conducted in which capillary tubes packed with ferrihydrite-coated glass spheres were injected with inorganic Fe(II) solutions under circumneutral pH conditions at 25 °C. Synchrotron X-ray diffraction was used to identify the secondary phase(s) formed and to provide data for quantitative kinetic analysis. At concentrations at and above 1.8 mM Fe(II) in the injection solution, magnetite was the only secondary phase formed (no intermediates were detected), with complete transformation following a nonlinear rate law requiring 28 and 150 h of reaction at 18 and 1.8 mM Fe(II), respectively. However, when the injection solution consisted of 0.36 mM Fe(II), goethite was the predominant reaction product and formed much more slowly according to a linear rate law, while only minor magnetite was formed. When the rates are normalized based on the time to react half of the ferrihydrite on a reduced time plot, it is apparent that the 1.8 mM and 18 mM input Fe(II) experiments can be described by the same reaction mechanism, while the 0.36 input Fe(II) experiment is distinct. The analysis of the transformation kinetics suggests that the transformations involved an electron transfer reaction between the aqueous as well as sorbed Fe(II) and ferrihydrite acting as a semiconductor, rather than a simple dissolution and recrystallization mechanism. A transformation mechanism involving sorbed inner sphere Fe(II) alone is not supported, since the essentially equal coverage of sorption sites in the 18 mM and 1.8 mM Fe(II) injections cannot explain the difference in the transformation rates observed.

Introduction

Iron oxy-hydroxides are abundant in subsurface environments and are important scavengers for a variety of nutrients and aqueous contaminants. In subsurface anoxic environments, the reduction of iron oxides by natural organic matter and by microbes is one of the most important processes for cycling of iron in the environment. The dissolved and sorbed ferrous iron (Fe(II)) produced during the reductive dissolution of iron oxides often controls the oxidation/reduction potential of anaerobic subsurface systems. Furthermore, the readsorption can cause structural changes in the host Fe-hydroxide minerals, potentially leading to the formation of such Fe(II)-bearing minerals as green rust and magnetite. Knowledge of the conditions under which Fe oxy-hydroxides transform, and the particular secondary phases they transform to, in the subsurface is very important for understanding their occurrence and for predicting the mobility of aqueous environmental contaminants that are influenced by these phases (*1*). However, little is known about the actual mechanisms and kinetics governing these transformation processes. Earlier studies indicated that the unstable Fe oxy-hydroxides phases, ferrihydrite and lepidocrocite, can convert to magnetite when reacted with ferrous ions in aqueous solutions (*2*−*4*). It was further postulated that green rust may be the intermediate phase during this phase transition process (*3*). However, later studies questioned the existence of such an intermediate phase, at least as a precursor to magnetite (*4*−*6*). There are also inconsistent reports on which transformation product formed in experiments conducted under similar conditions. Yee et al. (*6*) reported a transformation product of goethite only for the reaction of 2-line ferrihydrite with 100 mM Fe(II), which is inconsistent with the results of magnetite formation at much lower Fe(II) concentrations in the studies of Hansel et al. (*4*). Tronc et al. (*5*) reported the topotactic transformation of freshly synthesized 2-line ferrihydrite to magnetite as a result of mixing with Fe(II) solution, whereas Hansel et al. (*4*) attributed the transformation to magnetite mainly to nucleation and recrystallization. The exact mechanism and kinetics of the transformation, therefore, remain unclear.

Although a few column experiments have been conducted on anaerobic reductive transformations of Fe-oxyhydroxides (*7*, *8*), most of the studies conducted to date have been carried out in laboratory batch reactors where the primary objective was to qualitatively understand the conditions under which the transformations take place (*3*−*5*). However, the solution/solid ratios in most lab batch experiments are very different from those in actual subsurface microporous environments, especially under dynamic flow conditions where there is a continuous resupply of solution. One possibility is to study the transformation of ferrihydrite in conventional columns filled with natural sediments, but these have the disadvantage that the natural materials are characterized by significant chemical heterogeneities and thus are difficult to interpret. In this paper, a new capillary tube experimental setup was designed to simulate the reactions under dynamic flow conditions within a single well-controlled porous streamtube environment. Here we report on the kinetics of Fe(II)-catalyzed transformation of 6-line ferrihydrite under anaerobic flow conditions using this capillary tube experimental setup and synchrotron X-ray diffraction (XRD) solid phase characterization techniques.

Materials and Methods

All experiments were performed in an inert atmosphere (96% N_2/4% H_2) inside a laboratory anaerobic chamber (Plas Lab, Inc.) that was equipped with two palladium catalysts to remove trace oxygen at 25 °C. Oxygen free deionized water (18 MΩ·cm) was used in the preparation of all solutions.

* Corresponding author e-mail: LYang@lbl.gov; tel: 510-486-4774.
† Earth Sciences Division, Lawrence Berkeley National Laboratory.
‡ Advanced Light Source, Lawrence Berkeley National Laboratory.
§ Stanford Synchrotron Radiation Lightsource.

Experimental Setup and Procedure. Six-line ferrihydrite was synthesized following the method described by Schwertmann and Cornell (*9*) and was coated on uniformly sized microspheres of soda lime glass (72 μm nominal i.d., Duke Scientific, Inc.) before being used in the capillary tube experiment. Fused silica capillary tubing (SGE, Inc.) with an inner diameter of 110 μm and a wall thickness of 20 μm was used in the experiment as an analog of a single flow channel within microporous media. The extremely low gas permeability and chemical inertness of fused silica is well suited for the oxygen sensitive nature of the experiment, while allowing maximum transmission of synchrotron X-rays for sample analysis. For details of the capillary tube experimental system setup, see the Supporting Information. Three concentrations of ferrous sulfate solution, 0.36, 1.8, and 18 mM, buffered at pH of 6.8 with 10 mM PIPES, were used as injection solutions. The effluent collected at the other end was analyzed for solution chemistry by inductively coupled plasma mass spectrometry (ICP-MS, Perkin-Elmer DRCII) and a UV−vis spectrophotometer with ferrozine reagents. Preliminary experiments were conducted first to detect the first appearance of secondary minerals and bracket the reaction time required for complete transformations to take place at the three Fe(II) injection concentrations. Synchrotron X-ray diffraction pattern analysis was used as the primary means for monitoring the disappearance of 6-line ferrihydrite and concurrent growth of secondary mineral XRD peaks. X-ray absorption near edge spectroscopy (XANES) was also taken on the test samples to verify the completeness of the transformation. Based on the reaction time frame obtained, the capillary tube experiments were carried out so as to provide a time series of reacted samples, with each experiment designed to finish just before the start of synchrotron beam times so as to minimize time between the experiment and analysis. At the end of the specified reaction time, each reacted sample was thoroughly flushed with deoxygenated water for several hours before being disassembled inside the lab anaerobic chamber. The disassembled capillary samples were then sealed with epoxy at both ends and stored inside small anaerobic boxes equipped with anaerobic sachets (Mitsubishi) for transport to synchrotron beamlines for the sample analysis.

Sample Characterization and Analysis. Synchrotron X-ray diffraction analysis of the reacted samples was performed on beamline 10.3.2 at the Advanced Light Source (ALS) of Lawrence Berkeley National Laboratory and beamline 11.3 at the Stanford Synchrotron Radiation Lightsource (SSRL). A wavelength of 0.7293 (10.3.2) or 0.9578 (11.3) angstroms was used in the synchrotron XRD analysis of the samples. Both beamlines at ALS and SSRL are equipped with area detectors (CCD at 10.3.2; image plate at 11.3). The sample to detector distance and sample diffraction geometry during the experimental sample analysis were calibrated with either a lanthanum hexaboride (LaB_6, 11.3) or alumina (Al_2O_3, 10.3.2) standard. To correct for the drift of the incoming X-ray intensity from the storage ring, the readings on the ionization chamber (I_0) directly from incoming X-rays were used to normalize all the diffraction data. The two-dimensional diffraction image data acquired in this way were processed with the software Fit2D (*10*) to convert them to the traditional 2θ-intensity form. Further data processing and X-ray diffraction peak profile fittings were performed with the software Fullprof (*11*). A time series of samples was further characterized post-mortem with transmission electron microscopy at the National Center for Electron Microscopy (NCEM) of Lawrence Berkeley National Laboratory.

Results

Secondary Minerals and Effluent Chemistry. Synchrotron XRD analysis of the ferrihydrite-coated micrometer glass spheres showed 6 visible broad peaks corresponding very closely to 6-line ferrihydrite. When reacted with the 18 mM $FeSO_4$ injection solution, the ferrihydrite began to show visible peaks of magnetite after approximately 8 h of reaction. With the progress of the transformation reaction, magnetite peaks grew gradually along with the concurrent disappearance of ferrihydrite peaks, with complete transformation within 28 h. Magnetite was the only secondary mineral formed, as shown on the X-ray diffraction patterns of the time series of the reacted samples (Figure 1a). No green rust was detected in any of the experiments, despite the analysis of samples at early times. At 1.8 mM $FeSO_4$ injection, magnetite was still the only secondary mineral identified on the X-ray diffraction patterns, but it showed visible peaks of secondary magnetite

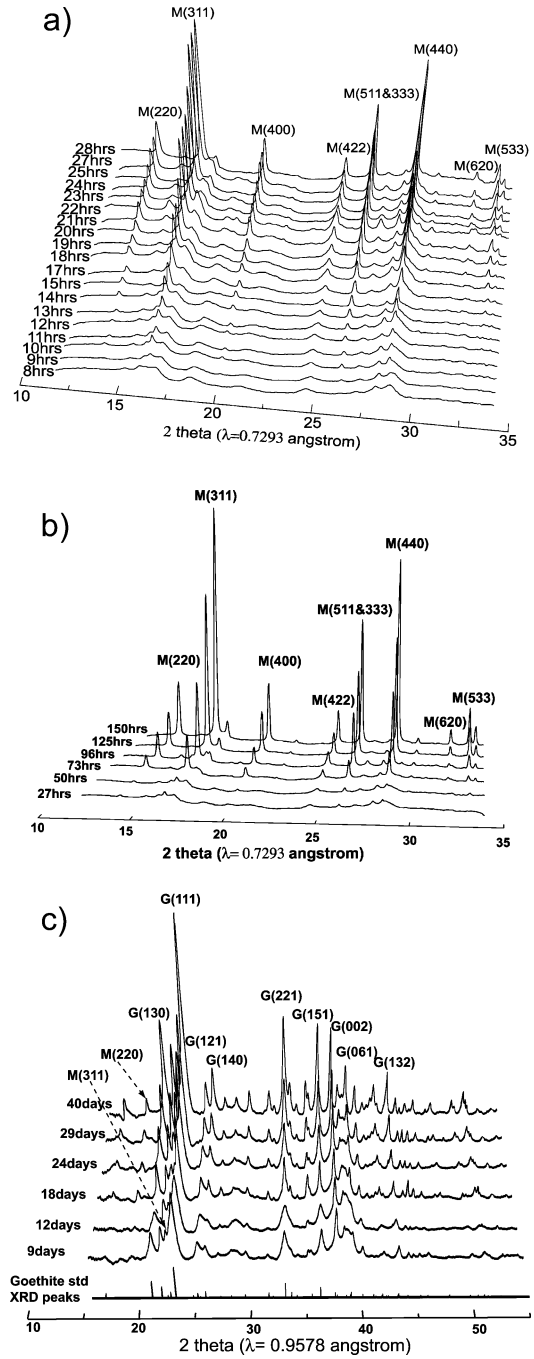

FIGURE 1. Time series of XRD patterns for ferrihydrite samples reacted with (a) 18 mM, (b) 1.8 mM, and (c) 0.36 mM ferrous sulfate solution. Labels are *hkl* index of goethite (G) and magnetite (M) XRD peaks. Goethite standard XRD peaks are also plotted for comparison in (c).

only after more than 12 h of reaction and it took approximately 150 h for complete transformation (Figure 1b). At 0.36 mM $FeSO_4$, transformation rates were considerably slower, with the development of initial visible X-ray diffraction peaks after approximately 9 days of reaction. There were still indications that magnetite formed, but only as weak discontinuous diffraction spots instead of continuous diffraction rings, indicating only minor amounts formed relative to the goethite. The principal secondary phase formed in this case was goethite (Figure 1c).

Chemical analysis of the effluent Fe by both ICP-MS and by the ferrozine method indicated that there was no detectable difference between the injection solution and the capillary tube effluent, with generally less than 1% variation for all three experimental conditions studied (for details, see SI). This indicates that no significant dissolution of ferrihydrite occurred. Although sorption of Fe(II) during the initial transient period would cause a slight drop in solution Fe concentration, such a decrease was not detected, likely due to the small amount of ferrihydrite inside the capillary tube used in this study.

Samples of ferrihydrite reacted with different concentrations of Fe(II) in the injection solution were also examined post-mortem using transmission electron microscopy (TEM) and selected area electron diffraction (SAED) to determine the occurrence and morphology of secondary minerals that formed. For samples reacted with 1.8 and 18 mM Fe(II), the only secondary mineral phase to be detected with TEM was magnetite, consistent with the synchrotron X-ray diffraction analysis results. In a time series of post-mortem samples examined under TEM, tiny magnetite seed crystals of about 7 nm were observed on the aggregates of ferrihydrite particles after about 11 h in the case of the 18 mM injection solution (SI, Figure S2a and b). At later stages of reaction, the magnetite particles grew considerably larger (up to 150 nm) and exhibited a hexagonal shaped morphology (SI, Figure S2c). For samples reacted with 0.36 mM Fe(II), most of the particles observed consisted of needle-shaped goethite with a particle size of 10−50 nm that grew out of ferrihydrite aggregates, with very few magnetite particles being observed (SI, Figure S2d).

Transformation Kinetics. The XRD patterns acquired on the time series of the reacted samples were further analyzed quantitatively to determine the kinetics of the transformation process. The integrated intensities of magnetite or goethite X-ray diffraction peaks in the time series of reacted samples were normalized against the value of the completely reacted samples to calculate the fractional transformation of secondary minerals. This provides a measure of the progress of the transformation reaction (the fractional conversion (α) ranging from 0 to 1). For samples reacted with 18 and 1.8 mM Fe(II) in the injection solution where magnetite was the only secondary mineral phase formed, the intensities of the weighted sum of the magnetite [311], [400], and [511]&[333] X-ray diffraction peaks were used to quantify reaction progress. For samples reacted with 0.36 mM Fe(II) where goethite was the dominant secondary phase formed (magnetite only constituted a very minor fraction of the total secondary mineral formed under these conditions), the intensities of goethite peaks only (the weighted sum of [110], [130], and [021] diffraction peaks) were used to quantify the extent of reaction. The intensities of magnetite and goethite X-ray diffraction peaks were calculated quantitatively by fitting the peaks in the diffraction patterns with pseudo-Voigt functions using the software Fullprof (*11*). These analyses provided the data for a plot of reaction time versus reaction progress (the extent of transformation) shown in Figure 2.

The experiments at 1.8 and 18 mM input Fe(II) showed a nonlinear transformation behavior of the ferrihydrite, with a slower rate of conversion at the beginning of the reaction that became more rapid at higher extents of reaction (Figure 2a and b). Only the samples reacted with 0.36 mM input Fe(II) showed a linear trend indicating a constant transformation rate (Figure 2c). A kinetic model for the transformation reaction can be expressed as:

$$\frac{1}{k}\frac{\partial \alpha}{\partial t} = f(\alpha) \tag{1}$$

where α represents the fractional conversion as defined above (i.e., the amount of product formed at reaction time t), t is the reaction time (induction time corrected), k is a temperature-dependent rate constant, $\partial\alpha/\partial t$ is the rate of conversion, and $f(\alpha)$ is a time-independent function of the converted fraction. Nonlinear fitting was performed on the kinetic $\alpha-t$ data collected on ferrihydrite samples reacted with 1.8 and 18 mM Fe(II) injections and it was found that the observed kinetic transformations can be described well with a power rate law in integrated form as:

$$\alpha = [k(t - t_0)]^2 \tag{2}$$

where t_0 is the induction time. The calculated rate constants, k, are $(1.31 \pm 0.055) \times 10^{-5}$ and $(2.14 \pm 0.052) \times 10^{-6}$ s^{-1} for 18 and 1.8 mM Fe(II) injection, respectively. Based on the data, the induction time, t_0, was determined to be 7.6 ± 0.65 and 14.2 ± 2.7 h for input Fe(II) concentrations of 18 and 1.8 mM respectively (Table 1).

The kinetic data for samples reacted with 0.36 mM Fe(II) were fitted very well with a linear kinetic rate law describing the transformation of ferrihydrite to goethite with the following equation:

$$\alpha = k(t - t_0) \tag{3}$$

The rate constant, k, obtained is $(3.12 \pm 0.15) \times 10^{-7}$ s^{-1} in this case and the induction time is estimated to be 98 ± 28.5 h (Table 1). To facilitate the comparison of kinetic data obtained under different experimental conditions, the kinetic data were plotted on an α versus reduced time, $(t - t_0)/(t_a - t_0)$, plot. In such a plot, a baseline time, t_a, is chosen for purposes of normalization. In this case, $t_{0.5}$, the time required for half of the total material (ferrihydrite) to react, was chosen as the baseline time. The result is a plot of the rate that is independent of the actual reaction rate and is characteristic of the reaction mechanism (*12*). When plotted in this fashion, it is clear that the transformation kinetics for the 1.8 and 18 mM Fe(II) experiments can be described with the same mechanism, despite the very different reaction rates and induction times determined (Figure 2d). The distinct reaction mechanism and order associated with the 0.36 mM Fe(II) injection experiment is also clear from this plot.

Discussion

As summarized by Cornell and Schwertmann (*13*), the transformations of iron oxides (hydroxides) can be structurally classified either as topotactic within a solid phase or as reconstructive in which the complete breakdown of the initial phase is followed by the crystallization of a new secondary phase.

Evaluation of Dissolution−Precipitation and Surface Adsorption/Precipitation Mechanisms. Because all the experiments were carried out at room temperature, pressure, and circumneutral pH conditions where reconstructive transformations might be expected to dominate (*13*), we consider first the possibility that a dissolution−precipitation mechanism is involved. Detailed examination of the data collected from this study, however, presents several arguments against a reconstructive mechanism. The first is based

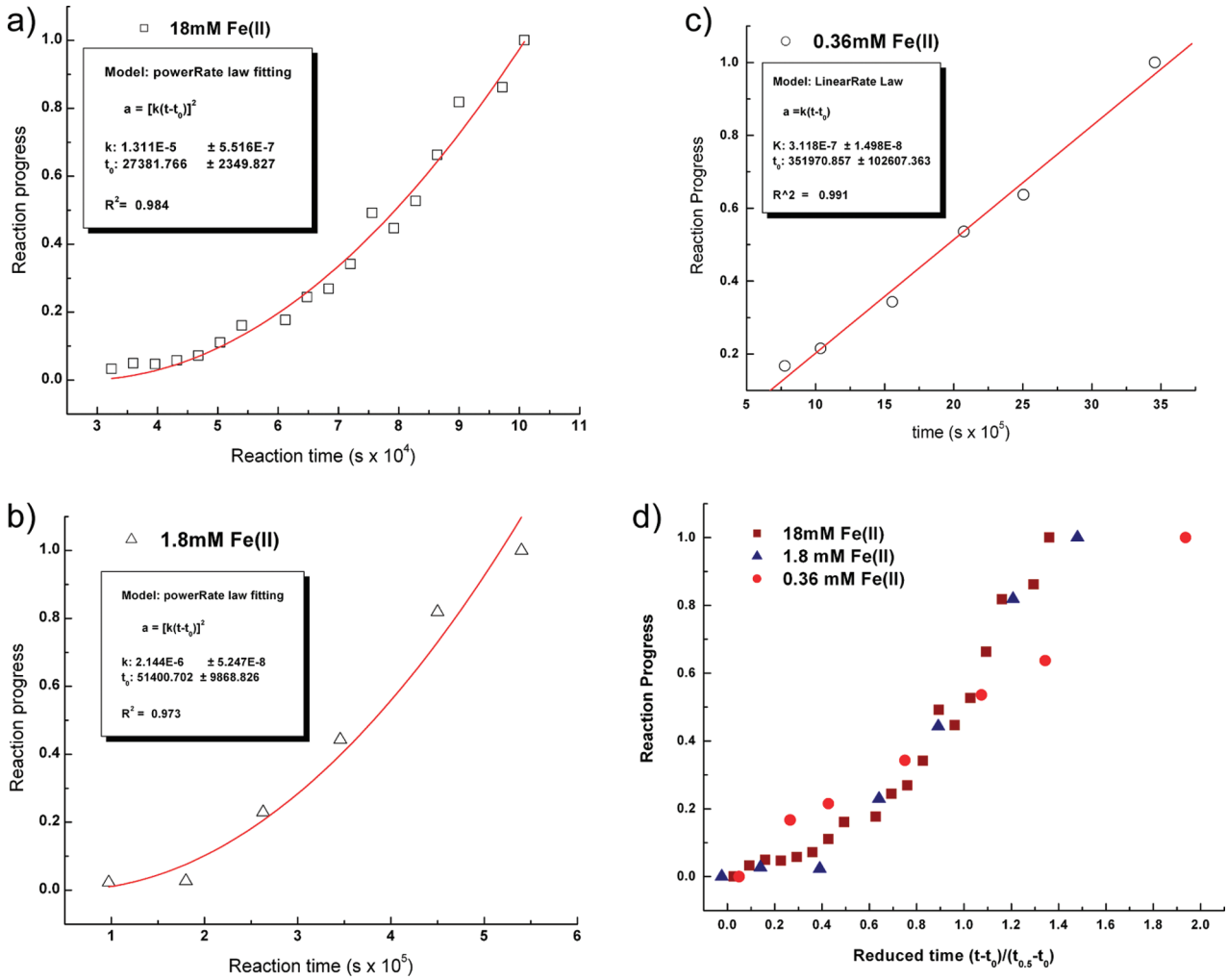

FIGURE 2. Kinetics of transformation process at (a) 18, (b) 1.8, and (c) 0.36 mM Fe(II) injection described by power rate and linear growth rate laws; (d) kinetics of transformation process on a reduced time graph (for a more detailed discussion, see text).

TABLE 1. Summary of the Transformation Pathways and Kinetic Models for the Reaction of 6-Line Ferrihydrite with Input Fe(II) Solutions at Experimental Conditions Studied (25 °C, pH 6.8)

	input Fe(II) concentration (mM)		
	18	1.8	0.36
Secondary minerals transformed	magnetite		goethite; trace magnetite
Kinetic models	$\alpha = [k(t - t_0)]^2$		$\alpha = k(t - t_0)$
Kinetic parameter k (s^{-1})	$1.31(\pm 0.055) \times 10^{-5}$	$2.14(\pm 0.052) \times 10^{-6}$	$3.12(\pm 0.15) \times 10^{-7}$
Induction time t_0 (h)	7.6 ± 0.65	14.2 ± 2.7	98 ± 28.5

on a comparison of the Gibbs energies of the two relevant phases, magnetite and goethite, at the experimental conditions. Compared to the Gibbs energy of 8.9 kJ/mol for goethite formation, magnetite formation has a Gibbs energy of 31.9, 35.3, and 39.3 kJ/mol for 0.36, 1.8, and 18 mM Fe(II) injection respectively (for details, see SI, Table S1). Magnetite should be strongly favored under all three input Fe(II) injections. Thus, it is very difficult to explain from a thermodynamic point of view why the dominant transformation product became goethite rather than magnetite given such a small change in Gibbs energy when input Fe(II) concentration decreased to 0.36 mM.

A second argument is based on the rate of ferrihydrite dissolution that would be required to explain the observations. From the time scale of the transformation reactions observed, the total Fe present in the capillary tube system and assuming a surface area of 600 m^2/g, the minimum dissolution rate of 6-line ferrihydrite is estimated to be 1.3 $\times 10^{-10}$ and 2.5×10^{-11} $mol/m^2/s$ for transformation taking place at 18 and 1.8 mM Fe(II) injections, respectively. These rates would be comparable to the reported values of ferrihydrite dissolution by strong reducing agents (such as 10 mM ascorbic acid) or microbially produced chelators (*14, 15*), and are too rapid for a system lacking such chelating agents at circumneutral pH and 25 °C. Furthermore, there was no statistically distinguishable difference between input and effluent solution Fe chemistry by ICP-MS analysis. Neither were there any signs of disintegration of the ferrihydrite coatings and accumulation at the downstream end of the capillary tubes due to such a rapid dissolution reaction.

For the magnetite formation observed in this study, another possible reaction mechanism is through oxidation and precipitation of the adsorbed ferrous ions on ferrihydrite particle surfaces via interfacial electron transfer reactions as suggested by Tronc et al. (*5*). The existence of such interfacial

electron transfer reactions between adsorbed Fe(II) and iron oxides has been experimentally confirmed by Williams and Scherer (*16*) and Larese-Casanova et al. (*17*) with Mossbauer spectroscopy. However, several observations argue against a mechanism relying *completely* on surface sorption, although this is not ruled out as one of the steps within the overall reaction mechanism. The ferrihydrite has a surface adsorption site density of 0.2 mol/mol Fe (*18*), which corresponds to about 2.8×10^{-8} mole of total sorption sites for the system studied here based on the total mass of ferrihydite inside the capillary tube system. Calculations of the Fe(II) adsorption on ferrihydrite using PHREEQC (*19*) and a two site surface complexation model based on the equilibrium constants from Appelo et al (*20*) indicate essentially the same surface coverage of strong binding sites by Fe(II) under all three experimental conditions studied (for details, see SI, Table S2). If surface adsorption of Fe(II) alone governed the rate of surface precipitation of magnetite, then magnetite should be observed under 0.36 mM Fe(II) injection conditions as well. There was also no distinguishable difference between the reacted and control samples when dissolving the Fe oxide coatings completely after the experiment. Moreover, such a surface precipitation model is difficult to reconcile with the observation that the transformation rates at 1.8 and 18 mM are higher with greater extents of reaction, since in this case one would expect rates to decrease as a magnetite layer progressively limits further adsorption of Fe(II) on the ferrihydrite surface.

Evaluation of a Mechanism Involving Electron Transfer Reaction between Semiconductor Ferrihydrite and the Fe(II)/Fe(III) Redox Couple in Solution. Iron oxides (hydroxides) are known semiconductors (*13, 21*). When a semiconductor is brought into contact with an electrolyte solution containing redox-active species, a charge transfer process will take place at the semiconductor−electrolyte interface if the Fermi level of the semiconductor (which represents the chemical potential of semiconductor electrons) is not in equilibrium with the electrochemical potential of the electrons in the electrolyte solution. This is a well-known phenomenon that has been extensively studied in the field of electrochemistry on semiconductors (*22, 23*). In the experimental system investigated in this study, the ferric irons produced from the dissolution of ferrihydrite will form a redox couple with the injected Fe(II) and could potentially cause an electron transfer reaction between the injecting Fe(II) solution and the semiconductor ferrihydrite.

The possibilities of such an electron transfer mechanism in the experimental system studied here are analyzed by comparing the electrochemical potential of the electrons in Fe(II)/Fe(III) redox couple and the Fermi level, as well as the absolute energy positions of conduction and valence bands of ferrihydrite mineral. As reviewed by Xu and Schoonen (*24*), the Fermi level and absolute energy positions of conduction and valence bands of pristine semiconductor minerals can be closely estimated using the method proposed by Bulter and Ginley (*25*). According to this method, the Fermi level energy of ferrihydrite can be calculated from the geometric mean of the electronegativities of its constituent atoms. Using the absolute electronegativities data on Fe, O, and H (*26*) and the suggested chemical formula of $Fe_{1.55}O_{1.66}(OH)_{1.34}$ for 6-line ferrrihydrite (*13*), the Fermi level energy of 6-line ferrihydrite is calculated to be 6.35 eV with respect to the absolute vacuum scale. Based on the band gap of 2.7 eV for ferrihydrite (*27*), the absolute energy of the conduction band minimum of ferrihydrite is calculated to be −5.00 eV. The electrochemical potentials of electrons in solution Fe(II)/Fe(III) redox couple can be calculated according to the Nernst equation using the concentrations of solution Fe(II) and Fe(III) and converted to the absolute energy by assuming the absolute energy of the standard hydrogen electrode (SHE) is −4.44 eV (*28*). However, the Fe(III) concentration in the effluent solution was undetectable by ICP-MS and colorimetric measurements. Lacking this, the Fe(III) concentrations in the effluent solution can only be estimated based on the solubility of ferrihydrite. Using a solubility product of $10^{-39.5}$ (*29*), the estimated absolute energy positions of the electrons at the Fe(II)/Fe(III) redox couple in the experiment systems are about −4.3 eV for all concentrations of Fe(II) injections (calculated using PHREEQC). It is possible that the electron transfer reactions may destabilize the ferrihydrite structure and promote the dissolution of ferrihydrite, which would potentially increase the solution Fe^{3+} concentration. However, there seems to be no significant increase in the ferrihydrite solubility due to such an effect based on the effluent chemistry analyses. Even assuming a 5 order magnitude increase in 6-line ferrihydrite solubility due to the Fe(II)-promoted dissolution, the estimated absolute energies were still around −4.6 eV for electrons in solution Fe(II)/Fe(III) redox couple at 0.36 mM Fe(II) injection. Those values were all above the Fermi level and conduction band energy of ferrihydrite. Such an energy difference between the electrons of solution Fe(II)/Fe(III) redox species and the Fermi level of ferrihydrite in the experimental system studied here would provide the continuous driving force for the electrons to be transferred from the electrolyte solution to the ferrihydrite, thus driving the ferrihydrite transformations. Although electron transfer reactions between solution electrolytes and semiconductor interfaces are very complex in detail, the simplified analysis presented above provides a general framework of the possible reactions that have happened in the experimental system studied.

Reaction Mechanisms for the Transformation Pathways Observed. The net effect of these electron injection reactions is the reductive disintegration of the ferrihydrite structure. The injected electrons can penetrate deep into the ferrihydrite particle and be trapped inside, thus destabilizing the ferrihydrite crystal and promoting its disintegration and the eventual release of the injected electron as a reduced Fe(II) species. Such penetration and trapping of injected electrons have been reported on colloidal hematite during electron transfer reactions with photosensitive dyes (*30, 31*). According to the theory of electron transfer reactions between semiconductor and electrolyte solutions, the injecting electron current density from the electron transfer reactions would vary under different concentrations of Fe(II) injections. We can qualitatively compare the experimental observations within the theoretical framework of electron transfer reactions between semiconductors and electrolyte solutions. As reviewed by Nozik and Memming et al. (*23*), the electron current density (j_c, A/cm^2) due to electron transfer from the electrolyte redox system to the conduction band of semiconductor in an ideal semiconductor−electrolyte interface is expressed as:

$$j_c = e k_c N_c C_{red} \quad (4)$$

where k_c is the electron transfer rate constant (cm^4 s^{-1}); e is the elementary charge of an electron (C); N_c is the density of the states at the bottom of conduction band (cm^{-3}); and C_{red} is the concentration of the reduced component in the redox couple (molecules cm^{-3}). Assuming the electron transfer rate and the density of the states at the bottom of ferrihydrite conduction band remain the same at all three Fe(II) injection conditions, eq 4 indicates that the injection electron current density would be higher at higher concentrations of Fe(II) in solution.

There are two scenarios depending on the electric current density of the injected electrons. If the electron current density is high and the destabilization of ferrihydrite to release

the structurally reduced Fe(II) is not fast enough to accommodate the injected electrons trapped inside, then magnetite can be formed through structural rearrangements of ferrihydrite into crystal nuclei of magnetite by olation-oxolation processes under solid state conditions. This is likely the case for the experiments using 1.8 and 18 mM injection $FeSO_4$ solution and is consistent with the observations of topotactic transformation of ferric hydroxide to magnetite catalyzed by aqueous Fe(II) in the study of Tronc et al. (*5*). This mechanism of magnetite transformation observed here is also in agreement with the solid state reduction of iron oxides into magnetite as observed by Stratmann et al. (*32, 33*) in electrochemical studies. Magnetite has an inverse-spinel structure and is highly electrically conductive due to the continuous exchange of the "extra" electrons between Fe^{2+} and Fe^{3+} in the octahedrally coordinated positions (*34*). Under the reaction mechanism proposed here, the reduced magnetite nuclei formed within the structure of ferrihydrite would further enhance electron injection into ferrihydrite particles from the surrounding electrolyte due to electron hopping between the Fe^{2+} and Fe^{3+} states. This would have the effect of accelerating the electron transfer reactions in the remaining ferrihydrite particles and explain the autocatalytic nonlinear kinetic behavior observed for the magnetite transformation at 1.8 and 18 mM. This interfacial electron transfer between colloidal magnetite and ferric hydroxide particles and the ensuing formation of reduced spinel layers on ferric hydroxide surfaces have been experimentally observed and confirmed by Belleville et al. (*35*). As outlined above, the injecting electron current density between the Fe(II) electrolyte solution and semiconductor ferrihydrite mineral would increase according to increasing solution Fe(II) concentration. This is qualitatively in agreement with the observation of the fastest magnetite conversion at the highest Fe(II) input concentration and consistent with the reaction mechanism described above.

In the case where the electron injection current density is low, however, the reductive disintegration of ferrihydrite would allow the injected electrons to be released as Fe(II) into surrounding electrolyte solution and promote its structure reconfiguration into more stable goethite through Ostwald ripening. This is likely the reaction mechanism for ferrihydrite reacting with 0.36 mM injection $FeSO_4$ solution. It is possible that the release of Fe(II) and transformation to goethite was a result of conduction through the bulk ferrihydrite and involved a series of redox-driven "conveyor belt" reactions as demonstrated in recent studies by Yania and Rosso, Handler et al., and Rosso et al. (*36*−*38*). The formation of magnetite in this case is likely to be accomplished by a more conventional heterogeneous nucleation and growth mechanism from the Fe(III) released during ferrihydrite structure breakdown and dissolution. The nature of the species released and the detailed steps involved during the transformation process, however, require further research. The kinetic behavior of transformation to goethite observed here agrees with the observations of Burleson and Penn (*39*), who studied the transformation of 6-line ferrihydrite nanoparticles to nanogoethite at neutral to alkaline conditions under elevated temperature. They reported a transformation of nano 6-line ferrihydrite into structures of goethite first, followed by linear growth of goethite through oriented aggregation. Instead of using high temperature to speed up the transformation process, as was done in the Burleson and Penn experiments, the transformation in this case was caused by electron transfer reactions from Fe(II) in solution. The overall reaction mechanisms and pathways proposed from the experiment findings in this study are illustrated in Figure 3.

Reconciliation of the Controversies in Previous Studies. The experimental observations obtained here are generally consistent with the experimental results on Fe(II)-catalyzed transformations of ferric hydroxides under similar conditions by other researchers (*4, 5, 40*). The induction times observed in this study are generally in accordance with the findings of Yee et al. (*6*) at ambient temperature when 2-line ferrihydrite was reacted with concentrated 100 mM Fe(II) solution. However, in their study, goethite was the only transformation product detected, in contrast to the observations from this study and those cited above. If the reaction involves an electron transfer reaction between Fe(II) in solution (not simply strongly surface adsorbed Fe(II)) and ferrihydrite, then the ratio of total Fe(II) in solution versus total Fe(III) available from ferrihydrite in the reaction system is also very important, since it will limit the total number of electrons that can be transferred per unit cell of ferrihydrite structure, and thus directly influence the secondary minerals formed. When the experimental systems used in the study of Hansel et al. (*4*) and Yee et al. (*6*) are examined carefully, the inconsistency of the results of these two studies can be explained by the very different solid/solution ratios used. Although the input Fe(II) concentration was much higher in the study of Yee et al. (*6*), a solid/solution (2-line ferrihydrite/Fe(II) solution) ratio of 1/136 was used in a closed batch reaction system according to their experimental description given. This only corresponds to a Fe(II)/Fe(III) of 0.7, which is similar to the Fe(II)/Fe(III) of 0.1−2.0 for the goethite formations observed in the studies of Hansel et al. (*4*) and Pedersen et al. (*40*). As noted by Yee et al. (*6*), magnetite was observed as the transformation product within 24 h when the Fe(II)/Fe(III) ratio increased 50 times, which would provide abundant ferrous ions needed for the electron transfer reactions between solution Fe(II)/Fe(III) redox species and the ferrihydrite mineral. The findings in this study point out the importance of semiconductor properties of iron oxide minerals and important role of the solid solution ratios in determining the reactions of iron oxides in anaerobic subsurface environments via an electron transfer mechanism.

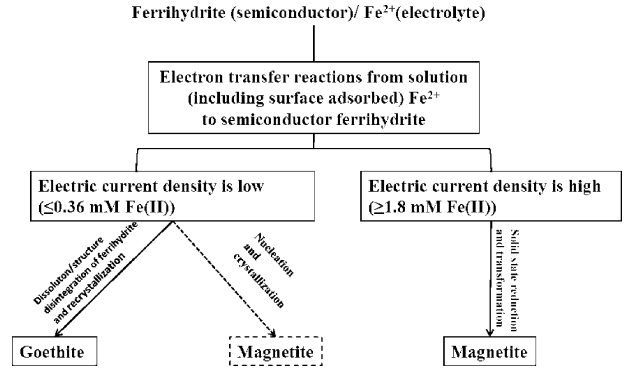

FIGURE 3. Reaction pathways and mechanisms proposed based on this study (solid lines indicate dominant pathways; dash lines indicate minor or less important reactions).

Acknowledgments

This research was funded by the U.S. Department of Energy's Environmental Remediation Science Program through a joint NSF−DOE Environmental Molecular Science Institute at Pennsylvania State University. We thank Xiangyun Song at EETD of LBNL and Sam Webb at SSRL for their help on TEM and synchrotron XRD analysis. The ALS is supported by the Director, Office of Science, Office of Basic Energy Sciences, of the U.S. DOE under contract DE-AC02-05CH11231. SSRL is a national user facility operated by Stanford University on behalf of the U.S. DOE Office of Basic Energy Sciences. The National Center for Electron Microscopy at LBNL is supported by the Office of Basic Energy Sciences, Material Sciences Division, of the U.S. DOE under contract DE-AC03-76SF00098.

Supporting Information Available

Details of the experimental setup, supporting figures, tables, and calculations referenced in this article. This information is available free of charge via the Internet at http://pubs.acs.org/.

Literature Cited

(1) Borch, T.; Kretzschmar, R.; Andreas Kappler, A.; Cappellen, P. V.; Ginder-Vogel, M.; Voegelin, A.; Campbell, A. Biogeochemical redox processes and their impact on contaminant dynamics. *Environ. Sci. Technol.* **2010**, *44*, 15–23.

(2) Ishikawa, T. Y.; Kondo, K.; Yasukawa, A.; Kandori, K. Formation of magnetite in the presence of ferric oxyhydroxides. *Corros. Sci.* **1998**, *40*, 1239–1251.

(3) Tamaura, Y.; Saturno, M.; Yamada, K.; Katsura, T. The transformation of γ-iron hydroxide oxide (γ-FeO(OH)) to iron oxide (Fe_3O_4) and green rust II in an aqueous solution. *Bull. Chem. Soc. Jpn.* **1984**, *57*, 2417–2421.

(4) Hansel, C. M.; Benner, S. G.; Fendorf, S. Competing Fe(II)-induced mineralization pathways of ferrihydrite. *Environ. Sci. Technol.* **2005**, *39*, 7147–7153.

(5) Tronc, E.; Belleville, P.; Jolivet, J. P.; Livage, J. Transformation of ferric hydroxide into spinel by Fe(II) adsorption. *Langmuir* **1992**, *8*, 313–319.

(6) Yee, N.; Shaw, S.; Benning, L.; Nguyen, T. H. The rate of ferrihydrite transformation to goethite via the Fe(II) pathway. *Am. Mineral.* **2006**, *91*, 92–96.

(7) Benner, S. G.; Hansel, C. M.; Wielinga, B. W.; Barber, T. M.; Fendorf, S. Reductive dissolution and biomineralization of iron hydroxide under dynamic flow conditions. *Environ. Sci. Technol.* **2002**, *36*, 1705–1711.

(8) Pallud, C.; Kausch, M.; Fendorf, S.; Meile, C. Spatial patterns and modeling of reductive ferrihydrite transformation observed in artificial soil aggregates. *Environ. Sci. Technol.* **2010**, *44*, 74–79.

(9) Schwertmann, U.; Cornell, R. M. *The Laboratory Synthesis of Iron Oxides*, 2nd ed.; Wiley-VCH: Weinheim, 2000.

(10) Hammersley, A. P.; Svensson, S. O.; Hanfland, M.; Fitch, A. N.; Häusermann, D. Two-dimensional detector software: from real detector to idealised image or two-theta scan. *High Pressure Res.* **1996**, *14*, 235–248.

(11) Rodríguez-Carvajal, J. Recent advances in magnetic structure determination by neutron powder diffraction. *Physica B: Condensed Matter* **1993**, *192*, 55–69.

(12) Brown, W. E.; Dollimore, D.; Galwey, A. K. Reactions in the solid state. In *Comprehensive Chemical Kinetics*; Bamford, C. H., Tipper, C. F. H., Eds.; Elsevier: New York, 1987.

(13) Cornell, R. M.; Schwertmann, U. *The Iron Oxides: Structure, Properties, Reactions, Occurrences, and Uses*, 2nd ed.; Wiley-VCH: Weinheim, 2003.

(14) Larsen, O.; Postma, D. Kinetics of reductive bulk dissolution of lepidocrocite, ferrihydrite, and goethite. *Geochim. Cosmochim. Acta* **2001**, *65*, 1367–1379.

(15) Dhungana, S.; Anthony, C. R., III; Hersman, L. Ferrihydrite dissolution by pyridine-2,6-bis(monothiocarboxylic acid) and hydrolysis products. *Geochim. Cosmochim. Acta* **2007**, *71*, 5651–5660.

(16) Williams, A. G. B.; Scherer, M. M. Spectroscopic evidence for Fe(II)-Fe(III) electron transfer at the iron oxide-water interface. *Environ. Sci. Technol.* **2004**, *38*, 4782–4790.

(17) Larese-Casanova, P.; Scherer, M. M. Fe(II) sorption on hematite: New insights based on spectroscopic measurements. *Environ. Sci. Technol.* **2007**, *41*, 471–477.

(18) Dzombak, D. A.; Morel, F. M. M. *Surface Complexation Modeling: Hydrous Ferric Oxide*; John Wiley: New York, 1990.

(19) Parkhurst, D. L.; Appelo, C. A. J. User's guide to PHREEQC (version 2)--A computer program for speciation, batch-reaction, one-dimensional transport, and inverse geochemical calculations. In *U.S. Geological Survey Water-Resources Investigations Report*; USGS: Denver, CO, 1999.

(20) Appelo, C. A. J.; Weiden Van Der, M. J. J.; Tournassat, C.; Charlet, L. Surface complexation of ferrous iron and carbonate on ferrihydrite and the mobilization of arsenic. *Environ. Sci. Technol.* **2002**, *36*, 3096–3103.

(21) Sherman, D. M. Electronic structures of iron(III) and manganese(IV) (hydr)oxide minerals: Thermodynamics of photochemical reductive dissolution in aquatic environments. *Geochim. Cosmochim. Acta* **2005**, *69*, 3249–3255.

(22) Koval, C. A.; Howard, J. N. Electron transfer at semiconductor electrode-liquid electrolyte interfaces. *Chem. Rev.* **1992**, *92*, 411–433.

(23) Nozik, A. J.; Memming, R. Physical chemistry of semiconductor-liquid interfaces. *J. Phys. Chem.* **1996**, *100*, 13061–13078.

(24) Xu, Y.; Schoonen, M. A. A. The absolute energy positions of conduction and valence bands of selected semiconducting minerals. *Am. Mineral.* **2000**, *85*, 543–556.

(25) Butler, M. A.; Ginley, D. S. Prediction of Flatband Potentials at Semiconductor-Electrolyte Interfaces from Atomic Electronegativities. *J. Electrochem. Soc.* **1978**, *125*, 228–232.

(26) Pearson, R. G. Absolute electronegativity and hardness: Application to inorganic chemistry. *Inorg. Chem.* **1988**, *27*, 734–740.

(27) Liu, G.; Debnath, S.; Paul, K. W.; Han, W.; Hausner, D. B.; Hosein, H.-A.; Michel, F. M.; Parise, J. B.; Sparks, D. L.; Strongin, D. R. Characterization and surface reactivity of ferrihydrite nanoparticles assembled in ferritin. *Langmuir* **2006**, *22*, 9313–9321.

(28) Trasatti, S. The abosolute electrode potential: an explanatory note. *Pure Appl. Chem.* **1986**, *58*, 955–966.

(29) Majzlan, J.; Navrotsky, A.; Schwertmann, U. Thermodynamics of iron oxides: Part III. Enthalpies of formation and stability of ferrihydrite ($Fe(OH)_3$), schwertmannite ($FeO(OH)_{3/4}(SO4)_{1/8}$) and ε-Fe_2O_3. *Geochim. Cosmochim. Acta* **2004**, *68*, 1049–1059.

(30) Dimitrijevic, N. M.; Savic, D.; Micic, O. I. Interfacial electron-transfer equilibria and flatband potentials of α-Fe_2O_3 and TiO_2 colloids studied by pulse radiolysis. *J. Phys. Chem.* **1984**, *88*, 4278–4283.

(31) Mulvaney, P.; Cooper, R.; Grieser, F.; Meisel, D. Charge trapping in the reductive dissolution of colloidal suspensions of iron(III) oxides. *Langmuir* **1988**, *4*, 1206–1211.

(32) Stratmann, M.; Bohnenkamp, K.; Engell, H. J. An electrochemical study of phase-transitions in rust layers. *Corros. Sci.* **1983**, *23*, 969–985.

(33) Stratmann, M.; Hoffmann, K. *In situ* Mossbauer spectroscopic study of reactions within rust layers. *Corros. Sci.* **1989**, *29*, 1329–1352.

(34) Fonin, M. S.; Dedkov, Y. S.; Pentcheva, R.; Rudiger, U.; Guntherodt, G. Magnetite: a search for the half-metallic state. *J. Phys: Condens. Matter* **2007**, *19*, 315217.

(35) Belleville, P.; Jolivet, J. P.; Tronc, E.; Livage, J. Crystallization of ferric hydroxide into spinel by adsorption on colloidal magnetite. *J. Colloid Interface Sci.* **1992**, *150*, 453–460.

(36) Yanina, S. V.; Rosso, K. M. Linked Reactivity at Mineral-Water Interfaces Through Bulk Crystal Conduction. *Science* **2008**, *320*, 218–222.

(37) Handler, R. M.; Beard, B. L.; Johnson, C. M.; Scherer, M. M. Atom exchange between aqueous Fe(II) and goethite: An Fe isotope tracer study. *Environ. Sci. Technol.* **2009**, *43*, 1102–1107.

(38) Rosso, K.; Yanina, S. V.; Gorski, C. A.; Larsese-casanova, P.; Scherer, M. M. Connecting observations of hematite (α-Fe_2O_3) growth catalyzed by Fe(II). *Environ. Sci. Technol.* **2010**, *44*, 61–67.

(39) Burleson, D. J.; Penn, R. L. Two-step growth of goethite from ferrihydrite. *Langmuir* **2006**, *22*, 402–409.

(40) Pedersen, H. D.; Postma, D.; Jakobsen, R.; Larsen, O. Fast transformation of iron oxyhydroxides by the catalytic action of aqueous Fe(II). *Geochim. Cosmochim. Acta* **2005**, *69*, 3967–3977.

ES1007565